Food Chemistry 287 (2019) 205–213

Contents lists available at ScienceDirect

Food Chemistry

journal homepage: www.elsevier.com/locate/foodchem

Simple and rapid detection of bisphenol A using a gold nanoparticle-based colorimetric aptasensor

Eun-Hee Lee[a,*], Sung Ku Lee[b], Min Jung Kim[c], Seung-Woo Lee[b,*]

[a] Department of Environmental Science and Engineering, Ewha Womans University, Seoul, Republic of Korea
[b] Department of Fine Chemistry, Seoul National University of Science and Technology, Seoul, Republic of Korea
[c] Research Group of Natural Materials and Metabolism, Korea Food Research Institute, Wanju-gun, Jeollabuk-do, Republic of Korea

ARTICLE INFO

Keywords:
Gold nanoparticles
Aptamer
Endocrine disruptor
Bisphenol A
Biosensor
Rice grain

ABSTRACT

A colorimetric aptasensor was developed for the simple and rapid detection of bisphenol A (BPA). The aptasensor was designed to consist of colloidal gold nanoparticles (AuNPs) and a BPA-specific 24-bp aptamer. The AuNP-aptamer conjugates underwent an electrolyte-induced aggregation in the presence of sub-ppb levels of BPA. The surface plasmon resonance shift of AuNPs facilitated a color change from red to blue upon aggregation, which was visually observed by the naked eye. The corresponding visual limit of detection of BPA was as low as 1 pg/mL (0.004 nM). The aptasensor also achieved a selective detection of BPA over a variety of BPA analogs. The applicability of the aptasensor was verified via a successful detection of BPA in a single grain of rice. This result indicates that the colorimetric aptasensor can be used in a screening procedure for food and environmental monitoring, with reliable performance to sub-ppb levels of BPA detection.

1. Introduction

Since the 1950s, bisphenol A (2,2-bis(4-hydroxyphenyl)propane, BPA) has been extensively used for manufacturing polycarbonate (PC) plastics and epoxy resins (i.e., polymeric coatings) because of its transparency and flame-retardant and thermal-resistant properties (Liao & Kannan, 2011). The commercial use of BPA has become ubiquitous, leading it to be commonly found in consumer products such as baby bottles, food and beverage containers, and thermal papers. The global consumption of BPA in 2016 was estimated to be 8 million metric tons, which corresponded to USD 16.4 billion ("Bisphenol-A, A global market overview," 2016). Such high volume and extensive use of BPA in plastics has resulted in its widespread detection in clinical, food, and water samples at low concentrations (Cao & Corriveau, 2008; Ehlert, Beumer, & Groot, 2008; Goodson, Robin, Summerfield, & Cooper, 2004; Lim, Kwack, Kim, Kim, & Lee, 2009; Park, Park, Jeong, Choi, & Kim, 2018; Spagnuolo, Marini, Sarabia, & Ortiz, 2017; Volkel, Kiranoglu, & Fromme, 2008).

The BPA leaching into food and environmental samples, specifically at the ppb levels, has recently raised concerns regarding food safety and environmental health (Alonso-Magdalena, Ropero, Soriano, Quesada, & Nadal, 2010; Liao & Kannan, 2011). The estimated daily intakes (EDIs) of BPA can be 0.007×10^{-4} μg/kg-body weight/day via migration from PC plastics to food simulants (Park et al., 2018). Due to ingestion of the BPA-exposed food, numerous monitoring studies have shown that BPA can be detected in human blood, tissues, serum, and urine (Vandenberg, Hauser, Marcus, Olea, & Welshons, 2007; Welshons, Nagel, & vom Saal, 2006; Lee et al., 2018b). BPA is considered to be an endocrine-disrupting compound that can interfere with hormone systems and functions by mimicking the actions of estrogen (Adoamnei et al., 2018; Diamanti-Kandarakis et al., 2009; Rubin, 2011). Moreover, urinary BPA concentrations in adults are associated with cardiovascular disease, impaired reproductive function, and even with diabetes (Mei et al., 2013). While there is scientific controversy surrounding the adverse health effects attributable to BPA, there is public support for banning the use of BPA in products due to its hazardous potential (Brewer & Ley, 2014). Human exposure to BPA caused by the consumption of contaminated food and drink has led to an increased demand for the detection and monitoring of BPA compound. Chromatographic analysis, including high-performance liquid chromatography (HPLC), liquid chromatography-mass spectrometry (LC-MS), and gas chromatography-mass spectrometry (GC–MS), and immunoassay-based analysis (e.g., ELISA) have been widely used for detecting BPA. Such techniques can provide excellent performance with high sensitivity and reproducibility for the detection of BPA (Ballesteros-Gomez, Rubio, & Perez-Bendito, 2009; Fernandez, André, & Cardeal, 2017; Wang et al., 2017). However, these analytical methods require advanced and expensive instrumentation as well as complicated, laborious, and time-

* Corresponding authors.
E-mail addresses: ehlee8102@gmail.com (E.-H. Lee), swlee@seoultech.ac.kr (S.-W. Lee).

https://doi.org/10.1016/j.foodchem.2019.02.079
Received 19 November 2018; Received in revised form 24 January 2019; Accepted 17 February 2019
Available online 23 February 2019

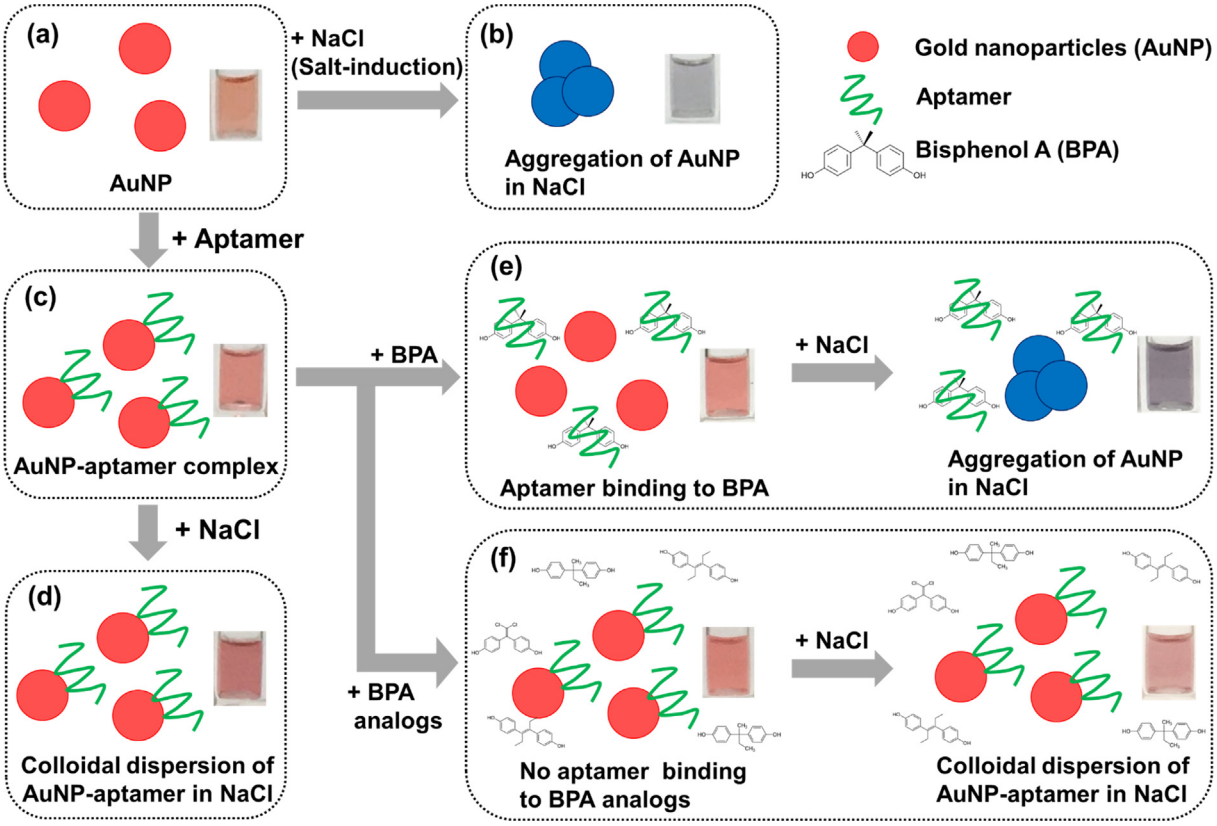

Fig. 1. Schematics of the colorimetric aptasensor for the detection of bisphenol A (BPA) via salt-induced aggregation. (a) Colloidal dispersion of the gold nanoparticles (AuNPs). (b) Electrolyte (NaCl)-induced aggregation of AuNPs. (c) Formation of AuNPs-aptamer complexes. (d) Dispersion of AuNP-aptamer complexes despite the addition of NaCl. (e) Aggregation of AuNP-aptamer complexes resulting from the binding of aptamer to BPA and the subsequent addition of NaCl. (f) Dispersion of AuNP-aptamer complexes in the presence of NaCl resulting from the low binding affinity of the aptamer to BPA analogs. Inset photographs of each box are the corresponding solutions.

consuming pre-treatment steps, which may hinder real-time and rapid analysis of BPA.

As an alternative, aptamer-based BPA detection in conjunction with various techniques, such as fluorescence spectrometry, colorimetry, electrochemistry, and surface-enhanced raman spectroscopy (SERS), has been proposed (Abnous, Danesh, Ramezani, Alibolandi, & Taghdisi, 2018; Baghayeri, Ansari, Nodehi, Razavipanah, & Veisi, 2018; He, Wang, Wang, Yu, & He, 2017; Jo et al., 2011; Kuang et al., 2014; Lee et al., 2018a; Lee, Lim, Lee, & Son, 2017; Mei et al., 2013; Zhou, Wang, Li, & Li, 2014). Aptamers are single-stranded oligonucleotide (e.g., ssRNA or ssDNA) molecules that are capable of binding target molecules with high affinity (Ilgu & Nilsen-Hamilton, 2016). Since their discovery in the 1990s, aptamers have shown several advantages such as simple synthesis, low cost, small size, and rapid response, which can provide flexibility, stability, sensitivity, and selectivity to the techniques. In this regard, these key features allow aptamers to be valuable tools by acting as sensory units for the development of improved analytical platforms that can satisfy market demands and analytical needs.

In this study, we present a simple and rapid screening method involving a colorimetric aptasensor based on colloidal gold nanoparticles (AuNPs) conjugated to a truncated BPA-specific 24-bp aptamer. The optical property of AuNP-aptamer complex influenced by the attractive and repulsive phenomena was used to afford a simple, rapid, and label-free detection of BPA without additional instrumental analysis. Due to the negative surface charge of aptamers, the conjugation of AuNPs with aptamers maintained a colloidal stability even in a high salt solution. On the other hand, the AuNP-aptamer complex was subjected to the aggregation upon the addition of BPA due to the affinity of aptamer towards BPA. The aggregation of AuNPs-aptamer complex introduced a significant surface plasmon resonance (SPR) shift that can be observed by the naked eye.

In order to balance the attractive and repulsive forces between the nanoparticles, the effective concentrations of electrolyte (i.e., NaCl) and aptamer were experimentally optimized in a series of tests for sub-ppb levels of BPA detection. Subsequently, we demonstrated the sensitivity and selectivity of the aptasensor by analyzing it with BPA and the various BPA analogs. Moreover, the applicability of the aptasensor was also validated by using it to detect BPA in a grain of rice. This analysis included visual identification of a color change upon introduction of a BPA-contaminated rice grain into the aptasensor.

2. Materials and methods

2.1. Reagents

Gold (III) chloride trihydrate ($HAuCl_4{\cdot}3H_2O$, ≥99.9%) and sodium citrate were purchased from Sigma-Aldrich (St. Louis, USA). Ultrapure distilled water (DNase/RNase/protease free) was obtained from iNtRON Biotechnology Inc. (Gyeonggi, Korea). BPA (> 99%), sodium chloride (NaCl, > 99.5%), and four BPA analogs (bisphenol B (BPB), bisphenol C (BPC), diphenolic acid (DPA), and bisphenol AF (BPAF)) were purchased from Daejung (Gyeonggi, Korea), Junsei Chemical Co. (Tokyo, Japan), and Tokyo Chemical Industry Co. (Tokyo, Japan), respectively.

2.2. Design of an aptamer specific for BPA

A single-stranded DNA (ssDNA) aptamer was designed for the development of a colorimetric aptasensor. Lee et al. previously reported a 24-mer ssDNA aptamer, 5′-TTT TTT TTT TGG ATA GCG GGT TCC-3′,

capable of detecting BPA with high sensitivity and selectivity (Lee et al., 2017). A slight variant of the reported aptamer, specifically modified to exclude the amine functional group at the 5′ terminus, was commercially synthesized (Bioneer Corporation, Daejeon, Korea), and then purified by carrying out polyacrylamide gel electrophoresis (PAGE).

2.3. Synthesis of AuNPs

Gold colloids were prepared using the traditional chemical reduction method (Turkevich, Stevenson, & Hillier, 1951). Briefly, a volume of 50 mL of a 1 mM $HAuCl_4{\cdot}3H_2O$ solution was transferred to a flask and heated until boiling under vigorous stirring. To this boiling solution, we added a volume of 5 mL of 38.8 mM sodium citrate, and the resulting mixture was kept boiling for 14 min. The resulting solution was cooled down to room temperature, and its volume was adjusted to 55 mL with distilled water. Gold colloids, with an average diameter of ~10 nm, formed in this solution and were stored at 4 °C prior to use.

2.4. Preparation of the colorimetric aptasensor

AuNP-aptamer complex for the colorimetric aptasensor were prepared as follows (see also Fig. 1). First, a volume of 230 μL of AuNP solution was transferred to each well of a clear 96-well microplate (Nunc™, Roskilde, Denmark). Subsequently, a volume of 20 μL of aptamer and NaCl solution was separately added to each of the wells of the microplate. Determinations of the optimum concentrations of NaCl and aptamer are described below in a Section 2.5. The microplate was subjected to an agitation at 500 rpm for 20 min at room temperature. After this incubation, the UV–Vis absorbance spectrum of the microplate containing solutions was acquired using a spectrofluorometer (Molecular Devices, SpectraMax M2, Sunnyvale, USA) over the wavelength range of 350–800 nm. The colorimetric changes of the AuNPs were normalized using the absorbances at 521 and 620 nm as follows (Mei et al., 2013):

$$Normalized\ absorbance = \frac{A620}{A521}$$

The AuNP solution was transferred to a 1.5-mL disposable cuvette for visual verification of the color change by the naked eye and optical photographs. All experiments were performed in triplicate. The same operating and measurement conditions were employed in the following experiments unless otherwise mentioned.

2.5. Optimization of NaCl and aptamer concentration for the colorimetric aptasensor

The optimum concentrations of NaCl and the aptamer for the colorimetric aptasensor were determined by acquiring and comparing absorbance spectra of solutions of AuNPs with various concentrations of aptamer and NaCl, respectively. First, volumes of 20 μL of solutions of various NaCl concentrations were added to wells of a clear 96-well microplate containing 230 μL of the AuNP solution to achieve final NaCl concentrations of 6.7, 13.3, 20.0, 26.7, 33.3, 40.0, 46.7, 53.3, 60.0, and 66.7 mM, respectively. Ultrapure distilled water was used as a negative control. The plate was incubated for 20 min, and the data for the absorbance spectrum and the normalized absorbance of each solution were acquired in the same manner described above in a Section 2.4. All experiments were performed in triplicate. As shown in Fig. 2a and 2b, a final concentration of 40.0 mM for NaCl was selected as the optimum concentration of NaCl for the colorimetric aptasensor.

Second, 20-μL aliquots of solutions of various concentrations of aptamer were separately added into wells of a clear 96-well microplate containing 230 μL of the AuNP solution to achieve desired aptamer concentrations of 0.03, 0.07, and 0.13 μM, respectively. The plate was incubated for 20 min, and then for each solution, we acquired its absorbance spectrum (Fig. 3a) and normalized absorbance (Fig. S2). Subsequently, each of these solutions was mixed with 20 μL of a NaCl solution to a final NaCl concentration of 40 mM. Followed by 20-min incubation after the NaCl addition, we acquired its absorbance spectrum (Fig. 3b) and normalized absorbance. All experiments were performed in triplicate. Based on these data, a final aptamer concentration of 0.13 μM was determined to be the optimum concentration for achieving rapid detection using the colorimetric aptasensor. Therefore, 0.13 μM of aptamer and 40 mM of NaCl were used in the following experiments unless otherwise stated.

2.6. Verification of the sensitivity and selectivity of the colorimetric aptasensor of BPA

The reaction solution used for validating the sensitivity and selectivity of the BPA detection was prepared in the same manner as described in the above sections detailing the preparation and optimization of the colorimetric aptasensor (Sections 2.4 and 2.5). For the sensitivity validation of the aptasensor, 30-μL aliquots of solutions of various concentrations of BPA were added to the plate to reach desired BPA concentrations of 0.001, 0.01, 0.1, 1, 10, 100, and 1000 ng/mL (equivalent to 0.004, 0.044, 0.44, 4.4, 43.8, 438, and 4380 nM). Ultrapure distilled water (i.e., no BPA added) was used as a negative control. The plate was incubated at 500 rpm for 20 min. Subsequently, a volume of 20 μL of a NaCl solution was added to the above solutions in the wells, followed by an incubation at 500 rpm for 20 min.

The selectivity of the colorimetric aptasensor was validated by analyzing chemical analogs of BPA. The target chemicals were added to samples of the solution to achieve desired concentrations of 1 ng/mL (equivalent to 4.4, 4.1, 3.6, 3.5, and 3.0 nM of BPA, BPB, BPC, DPA, and BPAF, respectively) and 1000 ng/mL (equivalent to 4380, 4128, 3557, 3492, and 2974 nM of BPA, BPB, BPC, DPA, and BPAF, respectively). BPA and ultrapure distilled water (i.e., no target chemical added) were used, respectively, as positive and negative controls. Four chemicals – BPA, BPC, DPA, and BPAF – were selected as structural analogs of BPA (Table S1). The absorbance spectra of the solutions were acquired, and their colors were visualized, in the same manners as were those described above. The normalized absorbance for each sample was determined as above. All experiments were performed in triplicate.

2.7. Detection of BPA in rice

Commercially available steamed rice (cooked white rice, CJ, Seoul, Korea) in a retort pouch was used to demonstrate the applicability of the aptasensor. Twenty-four grains (three grains per sample × four samples per experimental condition × two experimental conditions) of rice were prepared for exposure to distilled water or BPA. Specifically, half of the total rice (12 grains) was soaked in the distilled water for different durations, with three of the grains for 10 s, another three for 30 s, and the two other sets of three for 60 s and 300 s, respectively. At the same time, the other 12 grains of rice were immersed in 10 ng/mL (43.8 nM) BPA solutions, with three grains for each of 10, 30, 60, and 300 s as above. After the immersions, each grain of rice was transferred to a 96-well clear microplate containing the reaction solution. Note that the reaction solution was prepared in the same manner as described above. Thirty μL of ultrapure distilled water (a negative control) and 10 ng/mL (43.8 nM) BPA solution (a positive control) were separately added to wells of the microplate instead of grains of rice. The changes in optical property of the AuNP solution were verified by the UV–Vis measurement and the naked-eye observation. All experiments were performed in triplicate.

2.8. Scanning electron microscopic image analysis and zeta-potential measurement

The formation of AuNP aggregates was confirmed by scanning electron microscopic (SEM) image analysis. The AuNP aggregates were

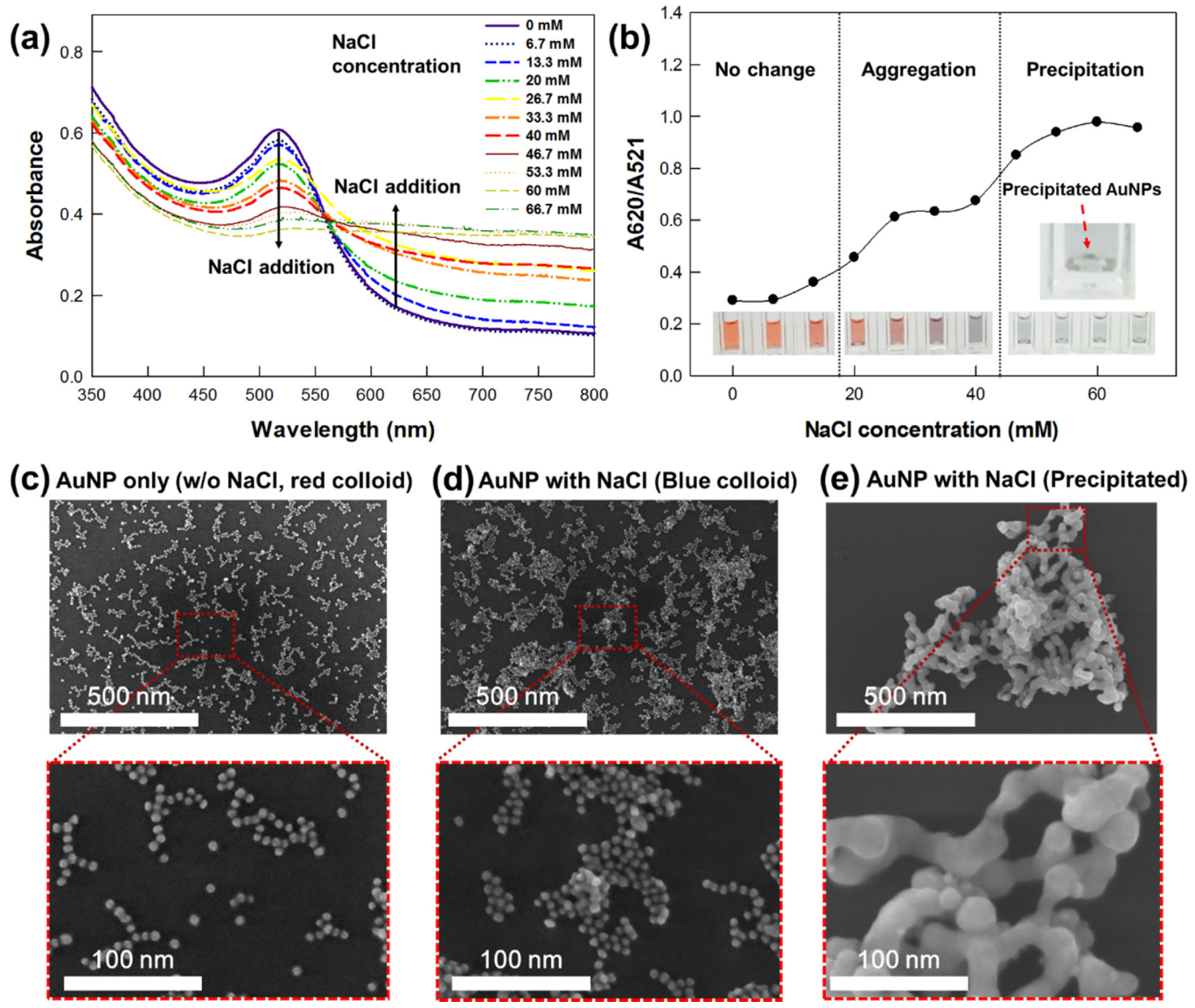

Fig. 2. Optimization of the NaCl concentration for salt-induced aggregation of colloidal gold nanoparticles (AuNPs). (a) UV–Vis absorbance spectra of colloidal AuNPs with various concentrations of NaCl. (b) Plot of the normalized absorbance (A620/A521) values of the AuNP solutions versus NaCl concentration. Inset photographs showing the color changes of the corresponding AuNP solutions. (c) Scanning electron microscope (SEM) images of the colloidal AuNPs. (d) SEM images of the AuNP aggregates upon addition of 40 mM NaCl. (e) SEM images of the precipitated AuNPs.

deposited onto a positively charged polyelectrolyte (Polyallylamine hydrochloride, 57.1 μM, Sigma-Aldrich)-coated silicon wafer (1 cm × 1 cm). After 10 min incubation, the silicon wafer was carefully washed with deionized water. The surface of AuNPs was viewed in field emission-scanning electron microscopy (FE-SEM, SU-70, Hitachi High Technologies Corp., Tokyo, Japan) with an accelerating voltage of 10 kV. Zeta potential (ζ) measurement was performed by laser Doppler velocimetry using zeta potential analyzer ELSZ-2000 (Otsuka Electronics, Osaka, Japan). Electrophoretic analysis was carried out in technical triplicates.

3. Results and discussion

3.1. Principle of the colorimetric aptasensor for sensitive and selective BPA detection

Fig. 1 shows the principle behind the colorimetric aptasensor for BPA detection. Four different conditions were simulated and examined to optimize the aptasensor consisted of AuNPs and a BPA-specific aptamer. Colloidal (unaggregated) AuNPs give a red color in solution due to the collective oscillation of particles' free electrons in the conduction band (Fig. 1a) (Wang & Sun, 2006). As the electrolyte salt (i.e., KCl or NaCl) was introduced to the dispersive AuNP solution, the AuNPs facilitated to be aggregated. The presence of the salt electrolytes in the AuNP solution decreased the inter-particle distance of AuNPs due to the screening of electrostatic repulsion between the charged AuNPs, thus the electromagnetic interaction among the adjacent AuNPs was introduced (Li & Rothberg, 2004). As a result, the color of the AuNP colloid gradually changes from burgundy to purple or blue (Fig. 1b) due to the cooperative association (e.g., Van der Waals attraction) of the colloidal AuNPs. In contrast, the immobilization of ssDNA aptamers on the AuNP surface, via attractive van der Waals forces between the bases in DNA and the AuNPs (Fig. 1c), stabilized the colloidal gold particles against salt-induced aggregation (Fig. 1d) (Li & Rothberg, 2004; Mei et al., 2013). On the other hand, the AuNP-aptamer complex did aggregate upon addition of BPA (Fig. 1e), resulting in the visual color change from red to purple. Such color changes can be attributed to the high affinity of the aptamer for BPA. Analysis of circular dichroism (CD)

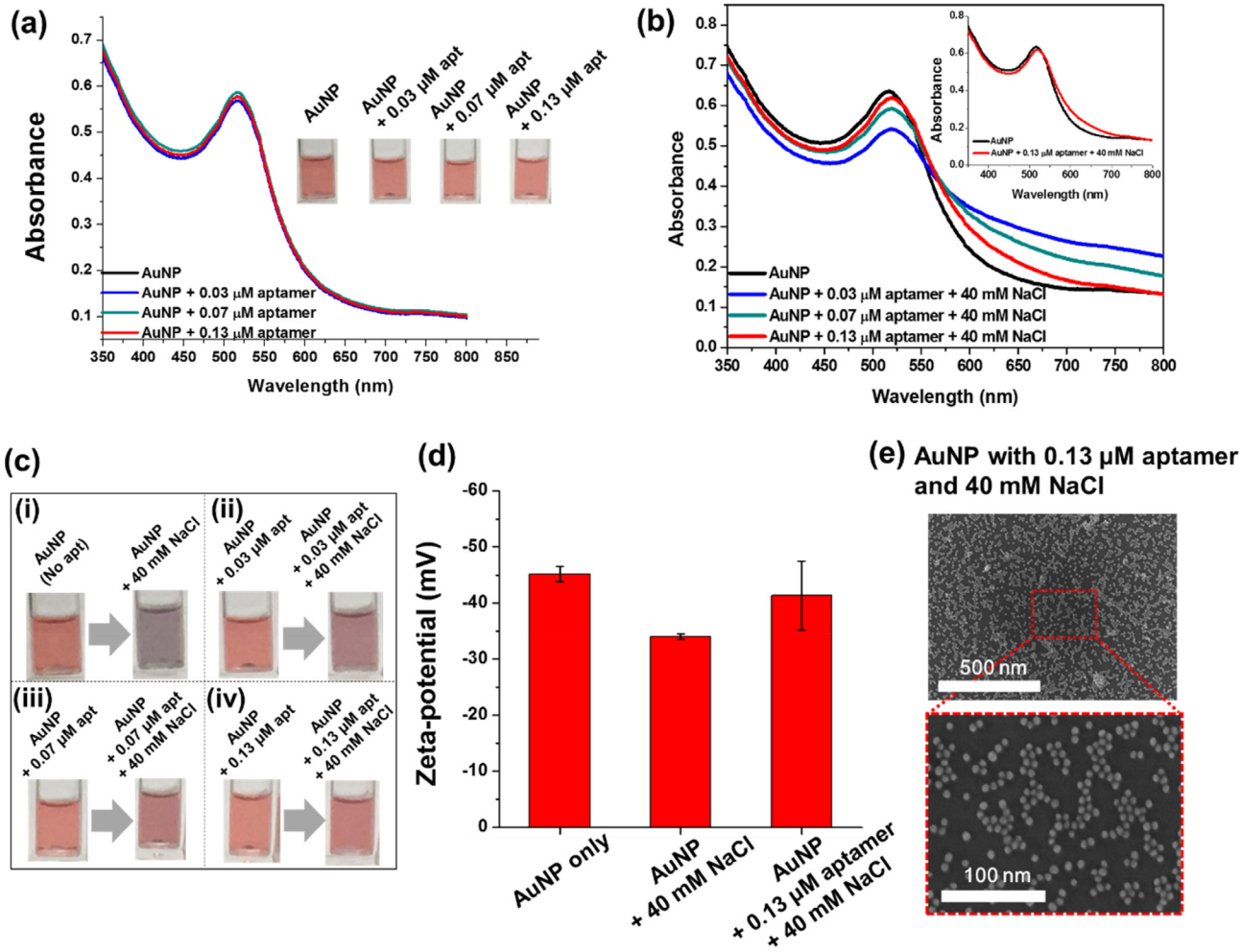

Fig. 3. Optimization of the aptamer concentration for the gold nanoparticle (AuNP)-aptamer conjugates. (a) UV–Vis spectra of AuNPs with various concentrations of aptamer. Inset photographs showing the visual color of the AuNP-aptamer complexes. (b) UV–Vis spectra changes of the AuNP-aptamer complexes via salt-induced aggregation. Inset showing absorbance spectrum of the AuNP with 0.13 μM aptamer in the presence of 40 mM NaCl compared with that of AuNP only. (c) Photographs showing visual color changes of various AuNP-aptamer conjugates with 40 mM NaCl. (d) Zeta-potentials of AuNP only, AuNP with 40 mM NaCl, and AuNP-aptamer conjugates with 40 mM NaCl. (e) Scanning electron microscope (SEM) images showing dispersion of the AuNP-aptamer complexes in the presence of NaCl.

spectra of the aptamer indicated that the aptamer underwent a conformational change upon coming into contact with BPA (Fig. S1). The conformational change of the aptamer was induced due to the aptamer binding to BPA, resulting in the subsequent release of the aptamer from the AuNPs (Li & Rothberg, 2004; Lee et al., 2018a; Xu et al., 2015). The repulsive force of the AuNP-aptamer complex was diminished by pulling off the aptamer from the AuNPs, making the AuNPs vulnerable to the salt-induced aggregation as described in Fig. 1e. The AuNPs-aptamer complex remained dispersed as colloidal particles in the presence of BPA analogs, due to the specificity of the aptamer for just BPA. Therefore, no significant color change was observed (Fig. 1f) even in the presence of the salt electrolyte.

3.2. Optimization of the salt-induced aggregation of gold nanoparticles

Controlling the salt-induced dispersion and aggregation of AuNPs is key for the success of an AuNP-based colorimetric sensor. For this purpose, our aptasensor was experimentally optimized with respect to two parameters, concentrations of NaCl and aptamer. The absorbance spectra in Fig. 2a show the optical property changes of AuNPs, for various NaCl concentrations. The colloidal AuNP solution exhibited a strong absorbance peak at 521 nm (marked by a solid purple line). Upon addition of NaCl, the aggregation of the AuNPs yielded a decrease in the height of this peak and an increase in the strength of absorbance at longer wavelengths (e.g., ~620 nm). The decrease in the intensity of 521 nm bands and the increase in the intensity of 620 nm bands indicated the formation of AuNP aggregates (Amendola, Pilot, Frasconi, Maragò, & Iatì, 2017; Li & Rothberg, 2004; Xu, Siriwardana, Zhou, Zou, & Zhang, 2018). The band broadening and shift in SPR depends on the particle size, shape, surface, and agglomeration state. The higher-order modes (i.e., dipole modes or multipolar modes) dominate at lower energy for larger AuNP aggregates (Amendola et al., 2017), resulting in the SPR band broadening and red-shifting. The redshift of the SPR band during aggregation of the AuNPs gave rise to a change in color from red to purple (or blue).

The normalized absorbance (A620/A521) increased marginally, from 0.29 to 0.36, as the NaCl concentration was increased from 0 to 13.3 mM, more rapidly to 0.85 as the NaCl concentration was increased further to 46.7 mM, and became saturated between levels of 0.85 and 0.96 at higher NaCl concentrations (Fig. 2b). The salt-induced AuNP aggregation was also visually confirmed by the change in color of the solution. As shown in Fig. 2b inset, the pristine AuNP colloids appeared to have a red color. As the NaCl concentration was increased from 0 to 13.3 mM, no obvious change in color was observed. However, when the NaCl concentration was increased to 26.7 mM, the solution turned dark red in color, indicating that AuNP aggregates probably began to form at

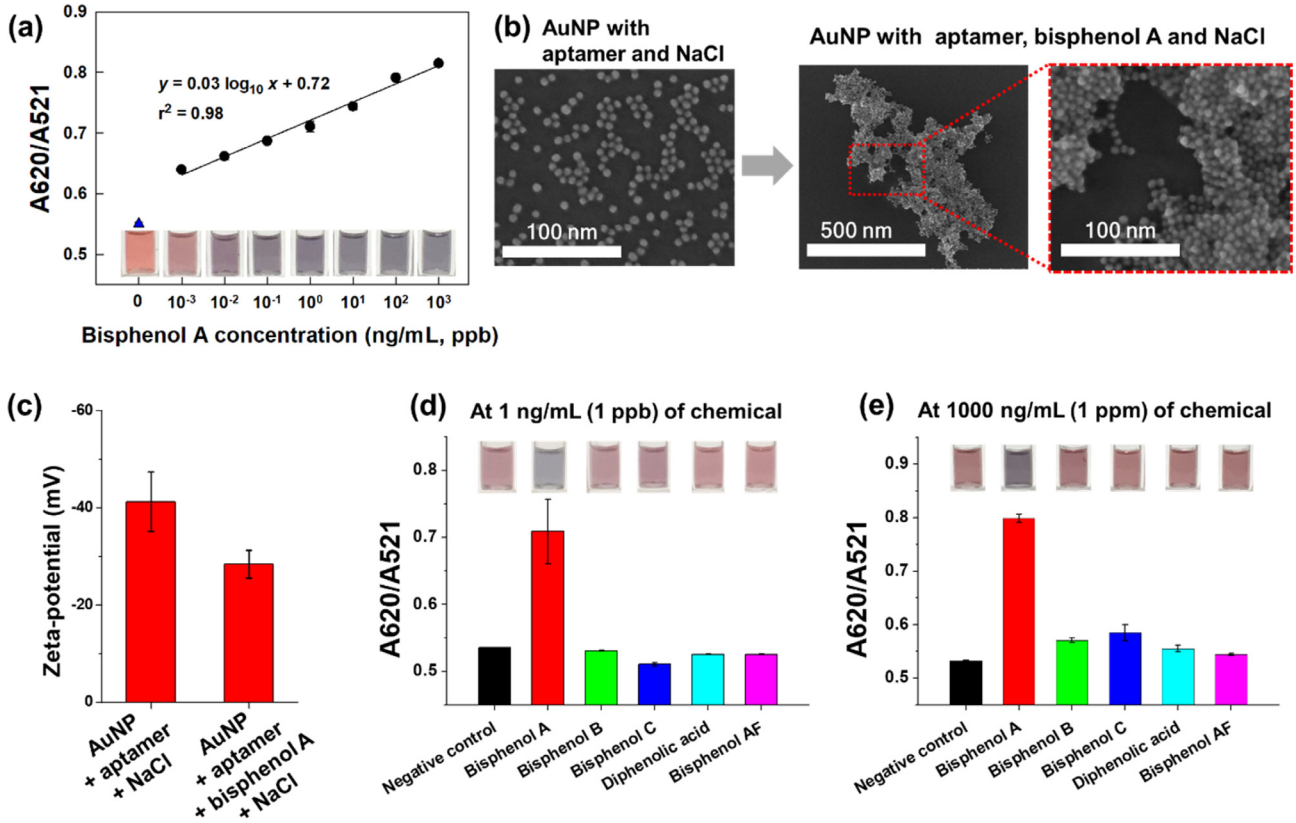

Fig. 4. Validation of the sensitivity and selectivity of the colorimetric aptasensor for bisphenol A (BPA) detection. (a) Normalized absorbance (A620/A521) values of gold nanoparticle (AuNP)-aptamer conjugate solutions at a range of 0.001–1000 ng/mL BPA (0.004–4380 nM). Blue triangle depicts the normalized absorbance of the solution with no BPA added (i.e., the negative control). Note that insets below the data points in the plot are photographs of the corresponding solutions of the AuNP-aptamer containing the indicated concentration of BPA. (b) Scanning electron microscope (SEM) images of AuNP-aptamer complexes before and after addition of BPA. (c) Zeta-potential changes of AuNPs-aptamer complexes upon addition of BPA. (d) Normalized absorbance values of solutions each containing AuNP-aptamer complexes and 1 ng/mL (4.4 nM) of the indicated target chemical. Insets above the bars are photographs of the corresponding solutions. (e) Normalized absorbance of solutions each containing AuNP-aptamer conjugates and 1000 ng/mL (4380 nM) of the indicated chemical. Insets above the bars are photographs of the corresponding solutions. (For interpretation of the references to color in this figure legend, the reader is referred to the web version of this article.)

this level of NaCl concentration. As the NaCl concentration was further increased to 40 mM, the color changes of the AuNP solution became purple or blue.

The marginal changes of the normalized absorbance at low NaCl concentrations were due to the low ionic strength of the electrolyte (presented in the section labeled as “No change” in Fig. 2b). In this region, not only the aggregation of AuNPs is slow, but also the mean size of the formed aggregates is closed to the nominal size of the original AuNPs (Wang & Sun, 2006). Thus, the color changes of the AuNPs were insignificant. However, in the region having higher ionic strength, the negative charges on the surface of AuNPs became strongly screened by the salt ions, so the attractive forces can act between the neighboring AuNPs (Chu, Han, Král, & Klajn, 2018), resulting in the subsequent aggregation (presented in the section labeled as “Aggregation” in Fig. 2b). It is worth noting that the AuNP colloid changed its color to even darker blue at concentrations above 40 mM NaCl. As the concentration further increased, the precipitation of AuNPs was also observed during the reaction, which resulted in a transparent solution (presented in a section labeled as “Precipitation” in Fig. 2b). The SEM images confirmed that the formation of AuNPs aggregates was increased with increasing salt concentration (Fig. 2c–e). The AuNP solution in the absence of NaCl (red colloid), no significant aggregation of the AuNPs was observed (Fig. 2c). In the presence of NaCl (< 40 mM), the small aggregates were observed in a blue AuNP colloid (Fig. 2d). The AuNP solution with access NaCl (> 50 mM), the large aggregates of AuNPs were formed (Fig. 2e). Strong precipitation of AuNPs at above 40 mM NaCl made the AuNP-based colorimetric sensors difficult to quantitatively distinguish the color change with the naked eye as well as with UV–Vis measurement. Thus, the higher concentrations above 40 mM NaCl were excluded as an optimum NaCl concentration despite of its high normalized absorbance level. In this study, 40 mM NaCl was selected to be the optimum concentration for the salt-induced aggregation of colloidal AuNPs.

3.3. Optimization of the formation of AuNP-aptamer conjugates

To determine the optimum concentration of the aptamer that can yield the highly sensitive detection of BPA, we first acquired absorbance spectra of solutions of AuNPs conjugated with various concentrations of the BPA-specific aptamer, from 0.03 to 0.13 μM (Fig. 3a). Note that conjugating aptamer into the AuNPs, at any of the concentrations tested, influenced neither the absorbance spectrum nor the visual color of the AuNP colloid (Fig. 3a). The normalized absorbance of the AuNPs upon conjugation with the aptamer remained at a value of 0.28–0.29 (Fig. S2), all of which showed insignificant differences from the AuNP only in both UV–Vis spectra and the naked eye observation (Fig. 3a). This result indicated that aptamer conjugation to AuNPs did not significantly influence the dispersion property of AuNPs.

As described in the schematics of the colorimetric aptasensor (Fig. 1c and 1d), the AuNPs with aptamer should not undergo the NaCl-induced aggregation in the absence of BPA. As 0.03 μM aptamer was conjugated to AuNPs, the substantial change of the absorbance spectrum of the AuNPs was observed after the addition of 40 mM NaCl (a blue line) compared with AuNP only (a black line, Fig. 3b). On the other

hand, the salt-induced aggregation of the AuNP-aptamer conjugates became less substantial upon increasing the concentration of aptamer from 0.03 to 0.13 μM. The conjugation of 0.13 μM aptamer into AuNPs achieved a spectrum similar to that of the pristine colloidal AuNP even after the addition of NaCl (inset of Fig. 3b). Correspondingly, the color changes of AuNP-aptamer complex in the presence of 40 mM NaCl were also visually observed as shown in Fig. 3c. As expected, 0.03 μM aptamer was insufficient to prevent the salt-induced aggregation of AuNPs, resulting in turned purple in color (Fig. 3c(ii)). On the other hand, the color of the AuNP solution with 0.13 μM aptamer was maginally changed upon addition of 40 mM NaCl (Fig. 3c(iv)).

The zeta-potential of AuNPs only was measured to be −45 mV, and it was decreased to −34 mV in the presence of 40 mM NaCl (Fig. 3d). Upon conjugation of 0.13 μM aptamer to AuNPs, the zeta-potential of the solution was −41 mV despite the presence of NaCl, indicating that the aptamer conjugation to the AuNP greatly diminished the salt-induced surface charge screening. The SEM analysis also confirmed that the AuNP-aptamer complex remained dispersed even in the salt electrolyte environment (Fig. 3e) similar to that of AuNP only (Fig. 2c). These results indicated that the addition of 0.13 μM aptamer to AuNPs effectively maintained the colloidal stability by preventing salt-induced aggregation. Therefore 0.13 μM aptamer was used.

3.4. Verification of the performance of the BPA aptasensor

The sensitivity of the colorimetric aptasensor was demonstrated over the BPA concentration range of 0.001–1000 ng/mL (equivalent to 0.004–4380 nM). The corresponding quantification curve and photographs of the resulting solutions are presented in Fig. 4a along with a negative control, i.e., having no target chemical (BPA) added, for comparison. As expected, the wavelength of the peak absorbance of AuNP-aptamer complex was red-shifted from 521 nm for the solution without any BPA to higher wavelengths upon inclusion of BPA (Fig. S3). Particularly, the considerable absorbance shift to a wavelength of 620 nm was observed when 1000 ng/mL (4380 nM) BPA was included. The normalized absorbance of the aptasensor was linearly proportional ($y = 0.03\ \log_{10} x + 0.72$, $r^2 = 0.98$) to the exponent of the concentration of BPA. Note that the normalized absorbance of the negative control (the solution without any BPA) at a value of ~0.55, was lower than the ~0.64 absorbance value of the solution with the lowest BPA concentration of 1 pg/mL (0.004 nM). This result was consistent with the changes in color shown in inset photographs of Fig. 4a. The addition of 1 pg/mL (0.004 nM) of BPA induced a color change of the AuNP-aptamer solution from red to purple, which was visible to the naked eye without any optical instrumentations. These results indicated that the designed AuNP-aptamer complex formed aggregates in the prescence of NaCl upon addition of BPA, which allowed us to quantify and detect BPA successfully even at a BPA concentration as low as 1 pg/mL (corresponding visual limit of detection (LOD), 1 ppt, 0.004 nM). As the BPA concentration was further increased, the color of the AuNP solution turned dark blue. The significant aggregation of AuNPs in the presence of BPA was also confirmed via SEM analysis (Fig. 4b). As described in the Section of 3.1 and 3.3, the AuNP-aptamer complex in the absence of BPA possessed strong dispersive force upon covering aptamers on AuNPs (Fig. 3e). As BPA was added to the aptasensor, the conformational change of the aptamer can occur due to the specific binding of the aptamer to BPA. This probably diminished the repulsive force of the AuNPs, resulting in the salt-induced formation of AuNP aggregates. The zeta-potential of the AuNP-aptamer complex upon addition of BPA was also decreased from −41 mV (i.e., no BPA added) to −28 mV in the presence of NaCl (Fig. 4c).

The selectivity of our aptasensor was demonstrated by testing it with chemical analogs of BPA (specifically, bisphenol B, bisphenol C, diphenolic acid, and bisphenol AF) as well as with BPA. The normalized absorbance increased only with BPA, by 32.4 ± 9.0% and 50.0 ± 1.4% at concentrations of 1 and 1000 ng/mL (4.4 and 4380 nM), respectively (Fig. 4d and 4e). On the other hand, the addition of the BPA analogs to the aptasensor resulted in neither any significant change in the absorbance spectrum nor in the normalized absorbance (Fig. S4). Note that the normalized absorbance differed by only between 2.1 ± 0.4 and 9.7 ± 2.9% upon addition of 1000 ng/mL BPA analogs (2974–4128 nM), compared with the negative control. As shown in the insets of Fig. 4d and e, the distinguishable color changes to blue were visually confirmed only in the solutions containing BPA, while the addition of the BPA analogs did not induce any apparent color changes in the AuNP solutions.

It is worth to note that our aptasensor was designed as a visible screening method for the simple and rapid detection of BPA in sub-ppb levels by the naked eye. The developed BPA-specific aptasensor exhibited the lower visual LOD of 1 pg/mL (0.004 nM) BPA, compared with spectroscopically measured values of 0.1 ng/mL BPA (0.44 nM) for label-free colorimetric aptasensor (Mei et al., 2013), 9 pg/mL (0.039 nM) BPA for a fluorescencing aptamer-gold nanosensor (Lee et al., 2018a), and 0.11 ng/mL (0.48 nM) BPA for a cysteamine-AuNP-based colorimetric aptasensor (Xu et al., 2015). The lower visual LOD is ascribed to the 24-bp truncated aptamer which was newly employed in our aptasensor (Lee et al., 2017). The 24-bp truncated BPA aptamer could significantly enhance performance for BPA detection than did 63-bp aptamer (Jo et al., 2011; Lee et al., 2017), since the shorter aptamer can provide better accessibility of BPA molecules to the AuNP-aptamer complex. The limit of visual detection of 1 pg/mL (0.004 nM) BPA for our aptasensor was lower than environmentally relevant BPA concentrations of 50–2280 pg/mL (0.219–9.99 nM, Guerra, Kim, Teslic, Alaee, & Smyth, 2015; Háková, Havlíková, Chvojka, Solich, & Šatínský, 2018; Kassotis et al., 2015), and the analytical result can be obtained with relatively simple operation. These attributes and results indicated that the developed aptasensor could fulfill the analytical requirements as a visual screening method for environmental and food samples.

3.5. Application of the aptasensor for the detection of BPA in rice

Lim et al. reported that the BPA migration level from a PC container to steamed rice was about 6–18 ng/mL (26.3–78.8 nM) when a PC bottle was heated to 100 °C for 9 min by a microwave oven (Lim et al., 2009), and 54.3 ng/mL (237.9 nM) of BPA was transferred from PC plastics to food simulants when it was treated in 50% ethanol at 70 °C (Park et al., 2018). Thus, the application of the colorimetric aptasensor was demonstrated by testing it with rice grains pre-treated with 10 ng/mL (43.8 nM) of BPA for different durations. As shown in Fig. 5a, the color of the AuNP solution turned from red to blue when BPA-treated rice grains were immersed in the aptasensor. Thirty seconds of the exposure of the rice grains to BPA even showed the slight color change. This change in color to blue became more obvious, when a duration of the exposure of the rice to BPA was increased from 30 to 300 s. Note that no significant visual color shift for rice grains soaked in distilled water. The normalized absorbance of the rice grains pre-treated with distilled water was sightly higher than the absorbance of the negative control. This was probably due to the effects of starch compounds from the rice grains. For the BPA-contaminated rice grains, the normalized absorbance was increased with increasing duration of BPA exposure (Fig. 5b). At a duration of the exposure of the rice to BPA of 300 s, the normalized absorbance was 0.71, and it was similar to that of the positive control (i.e., with 10 ng/mL (43.8 nM) of BPA solution added, 0.73).

4. Conclusions

We demonstrated a simple, rapid, and label-free colorimetric aptasensor for sensitive and selective BPA detection at sub-ppb levels. The performance of colorimetric aptasensor was confirmed by spectral changes, photographic and SEM image analysis, and zeta-potential measurements. We were able to successfully use the aptasensor to

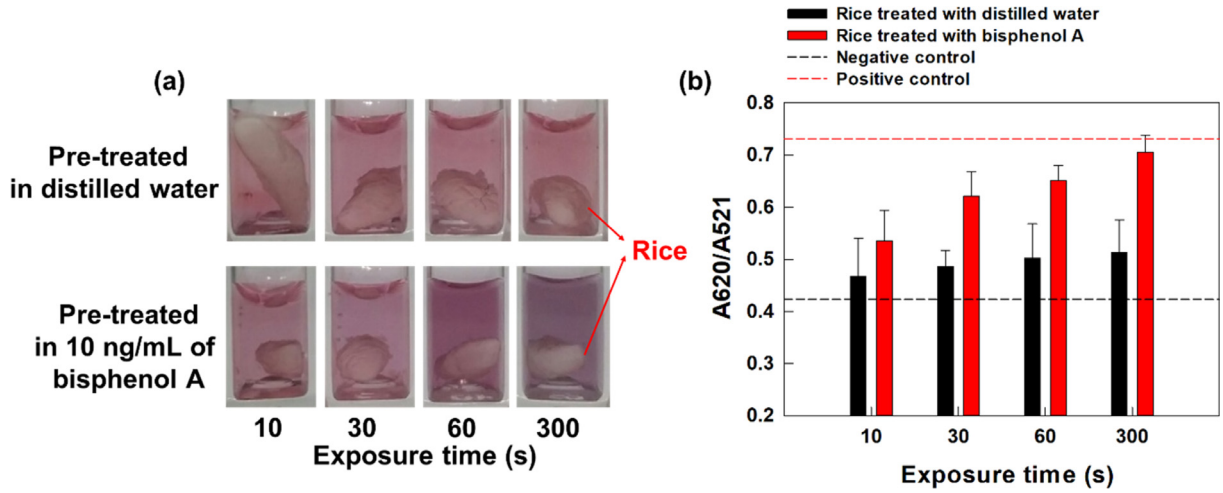

Fig. 5. Detection of bisphenol A (BPA) in steamed rice. (a) Photographs of the gold nanoparticle (AuNP) solutions each with a grain of rice treated with BPA or distilled water (DW) for the indicated duration. (b) Normalized absorbance (A620/A521) values of the colorimetric aptasensor in the presence of individual grains of rice, each treated with BPA or DW for the indicated duration. Black and red dotted lines in panel b represent results for the aptasensor with DW and 10 ng/mL (43.8 nM) of BPA solution added, i.e., negative and positive controls, respectively. (For interpretation of the references to color in this figure legend, the reader is referred to the web version of this article.)

visually detect BPA in a single grain of steamed rice that was exposed to BPA for as little as 30 s. The information gained in this study suggests that the colorimetric aptasensor has shown comparable performance to chromatographic- and immunoassay-based instrumental analysis, and has the potential to satisfy the analytical needs for the rapid detection of BPA in food and environmental samples.

Declaration of interests

The authors declare that they have no known competing financial interests or personal relationships that could have appeared to influence the work reported in this paper.

Acknowledgments

This study was supported by the research program funded by the SEOULTECH (Seoul National University of Science and Technology, Research Fund for the new faculty), and in part funded by the National Research Foundation of Korea (NRF) grant funded by the Korean government (NRF-2017R1A2B4003507) and by internal program of Korea Food Research Institute (KFRI, E0170100).

Appendix A. Supplementary data

Supplementary data to this article can be found online at https://doi.org/10.1016/j.foodchem.2019.02.079.

References

Abnous, K., Danesh, N. M., Ramezani, M., Alibolandi, M., & Taghdisi, S. M. (2018). A novel electrochemical sensor for bisphenol A detection based on nontarget-induced extension of aptamer length and formation of a physical barrier. *Biosensors and Bioelectronics, 119*, 204–208.

Adoamnei, E., Mendiola, J., Vela-Soria, F., Fernández, M. F., Olea, N., Jørgensen, N., ... Torres-Cantero, A. M. (2018). Urinary bisphenol A concentrations are associated with reproductive parameters in young men. *Environmental Research, 161*, 122–128.

Alonso-Magdalena, P., Ropero, A. B., Soriano, S., Quesada, I., & Nadal, A. (2010). Bisphenol-A: A new diabetogenic factor? *Hormones-International Journal of Endocrinology and Metabolism, 9*(2), 118–126.

Amendola, V., Pilot, R., Frasconi, M., Maragò, O. M., & Iatì, M. A. (2017). Surface plasmon resonance in gold nanoparticles: A review. *Journal of Physics: Condensed Matter, 29*(20), 203002.

Baghayeri, M., Ansari, R., Nodehi, M., Razavipanah, I., & Veisi, H. (2018). Label-free electrochemical bisphenol A aptasensor based on designing and fabrication of a magnetic gold nanocomposite. *Electroanalysis, 30*(9), 2160–2166.

Ballesteros-Gomez, A., Rubio, S., & Perez-Bendito, D. (2009). Analytical methods for the determination of bisphenol A in food. *Journal of Chromatography A, 1216*(3), 449–469.

Bisphenol-A (2016). A global market overview. Industry Experts, Hyderabad, India.

Brewer, P. R., & Ley, B. L. (2014). Contested evidence: Exposure to competing scientific claims and public support for banning bisphenol A. *Public Understanding of Science, 23*(4), 395–410.

Cao, X. L., & Corriveau, J. (2008). Migration of bisphenol A from polycarbonate baby and water bottles into water under severe conditions. *Journal of Agricultural and Food Chemistry, 56*(15), 6378–6381.

Chu, Z., Han, Y., Král, P., & Klajn, R. (2018). "Precipitation on Nanoparticles": Attractive intermolecular interactions stabilize specific ligand ratios on the surfaces of nanoparticles. *Angewandte Chemie International Edition, 57*(24), 7023–7027.

Diamanti-Kandarakis, E., Bourguignon, J. P., Giudice, L. C., Hauser, R., Prins, G. S., Soto, A. M., ... Gore, A. C. (2009). Endocrine-disrupting chemicals: An endocrine society scientific statement. *Endocrine Reviews, 30*(4), 293–342.

Ehlert, K. A., Beumer, C. W. E., & Groot, M. C. E. (2008). Migration of bisphenol A into water from polycarbonate baby bottles during microwave heating. *Food Additives and Contaminants Part a-Chemistry Analysis Control Exposure & Risk Assessment, 25*(7), 904–910.

Fernandez, M. A. M., André, L. C., & Cardeal, Z. de L. (2017). Hollow fiber liquid-phase microextraction-gas chromatography-mass spectrometry method to analyze bisphenol A and other plasticizer metabolites. *Journal of Chromatography A, 1481*, 31–36.

Goodson, A., Robin, H., Summerfield, W., & Cooper, I. (2004). Migration of bisphenol A from can coatings – effects of damage, storage conditions and heating. *Food Additives and Contaminants, 21*(10), 1015–1026.

Guerra, P., Kim, M., Teslic, S., Alaee, M., & Smyth, S. A. (2015). Bisphenol-A removal in various wastewater treatment processes: Operational conditions, mass balance, and optimization. *Journal of Environmental Management, 152*, 192–200.

Háková, M., Havlíková, L. C., Chvojka, J., Solich, P., & Šatínský, D. (2018). An on-line coupling of nanofibrous extraction with column-switching high performance liquid chromatography – A case study on the determination of bisphenol A in environmental water samples. *Talanta, 178*, 141–146.

He, M. Q., Wang, K., Wang, J., Yu, Y. L., & He, R. H. (2017). A sensitive aptasensor based on molybdenum carbide nanotubes and label-free aptamer for detection of bisphenol A. *Analytical and Bioanalytical Chemistry, 409*(7), 1797–1803.

Ilgu, M., & Nilsen-Hamilton, M. (2016). Aptamers in analytics. *Analyst, 141*(5), 1551–1568.

Jo, M., Ahn, J. Y., Lee, J., Lee, S., Hong, S. W., Yoo, J. W., ... Kim, S. (2011). Development of single-stranded DNA aptamers for specific Bisphenol a detection. *Oligonucleotides, 21*(2), 85–91.

Kassotis, C. D., Alvarez, D. A., Taylor, J. A., vom Saal, F. S., Nagel, S. C., & Tillitt, D. E. (2015). Characterization of Missouri surface waters near point sources of pollution reveals potential novel atmospheric route of exposure for bisphenol A and wastewater hormonal activity pattern. *Science of the Total Environment, 524–525*, 384–393.

Kuang, H., Yin, H., Liu, L., Xu, L., Ma, W., & Xu, C. (2014). Asymmetric plasmonic aptasensor for sensitive detection of bisphenol A. *ACS Applied Materials & Interfaces, 6*(1), 364–369.

Lee, E. H., Lim, H. J., Lee, S. D., & Son, A. (2017). Highly sensitive detection of bisphenol A by NanoAptamer assay with truncated aptamer. *ACS Applied Materials & Interfaces, 9*(17), 14889–14898.

Lee, E. S., Kim, G. B., Ryu, S. H., Kim, H., Yoo, H. H., Yoon, M. Y., ... Kim, Y. P. (2018a). Fluorescing aptamer-gold nanosensors for enhanced sensitivity to bisphenol A. *Sensors and Actuators B: Chemical, 260*, 371–379.

Lee, J., Choi, K., Park, J., Moon, H. B., Choi, G., Lee, J. J., ... Kim, S. (2018b). Bisphenol A

distribution in serum, urine, placenta, breast milk, and umbilical cord serum in a birth panel of mother–neonate pairs. *Science of The Total Environment, 626*, 1494–1501.
Li, H., & Rothberg, L. (2004). Colorimetric detection of DNA sequences based on electrostatic interactions with unmodified gold nanoparticles. *Proceedings of the National Academy of Sciences of the United States of America, 101*(39), 14036–14039.
Liao, C. Y., & Kannan, K. (2011). Widespread occurrence of bisphenol A in paper and paper products: Implications for human exposure. *Environmental Science & Technology, 45*(21), 9372–9379.
Lim, D. S., Kwack, S. J., Kim, K. B., Kim, H. S., & Lee, B. M. (2009). Potential risk of bisphenol A migration from polycarbonate containers after heating, boiling, and microwaving. *Journal of Toxicology and Environmental Health-Part a-Current Issues, 72*(21–22), 1285–1291.
Mei, Z. L., Chu, H., Chen, W., Xue, F., Liu, J., Xu, H., ... Zheng, L. (2013). Ultrasensitive one-step rapid visual detection of bisphenol A in water samples by label-free aptasensor. *Biosensors and Bioelectronics, 39*(1), 26–30.
Park, S. R., Park, S. J., Jeong, M. J., Choi, J. C., & Kim, M. K. (2018). Fast and simple determination and exposure assessment of bisphenol A, phenol, *p*-tert-butylphenol, and diphenyl carbonate transferred from polycarbonate food-contact materials to food simulants. *Chemosphere, 203*, 300–306.
Rubin, B. S. (2011). Bisphenol A: An endocrine disruptor with widespread exposure and multiple effects. *Journal of Steroid Biochemistry and Molecular Biology, 127*(1–2), 27–34.
Spagnuolo, M. L., Marini, F., Sarabia, L. A., & Ortiz, M. C. (2017). Migration test of bisphenol A from polycarbonate cups using excitation-emission fluorescence data with parallel factor analysis. *Talanta, 167*, 367–378.
Turkevich, J., Stevenson, P. C., & Hillier, J. (1951). A study of the nucleation and growth processes in the synthesis of colloidal gold. *Discussions of the Faraday Society, 11*, 55–75.
Vandenberg, L. N., Hauser, R., Marcus, M., Olea, N., & Welshons, W. V. (2007). Human exposure to bisphenol A (BPA). *Reproductive Toxicology, 24*(2), 139–177.
Volkel, W., Kiranoglu, M., & Fromme, H. (2008). Determination of free and total bisphenol A in human urine to assess daily uptake as a basis for a valid risk assessment. *Toxicology Letters, 179*(3), 155–162.
Wang, G., & Sun, W. F. (2006). Optical limiting of gold nanoparticle aggregates induced by electrolytes. *Journal of Physical Chemistry B, 110*(42), 20901–20905.
Wang, Q., Zhu, L., Chen, M., Ma, X., Wang, X., & Xia, J. (2017). Simultaneously determination of bisphenol A and its alternatives in sediment by ultrasound-assisted and solid phase extractions followed by derivatization using GC-MS. *Chemosphere, 169*, 709–715.
Welshons, W. V., Nagel, S. C., & vom Saal, F. S. (2006). Large effects from small exposures. III. Endocrine mechanisms mediating effects of bisphenol A at levels of human exposure. *Endocrinology, 147*(6), S56–S69.
Xu, J., Li, Y., Bie, J., Jiang, W., Guo, J., Luo, Y., ... Sun, C. (2015). Colorimetric method for determination of bisphenol A based on aptamer-mediated aggregation of positively charged gold nanoparticles. *Microchimica Acta, 182*(13), 2131–2138.
Xu, J. X., Siriwardana, K., Zhou, Y., Zou, S., & Zhang, D. (2018). Quantification of gold nanoparticle ultraviolet-visible extinction, absorption, and scattering cross-section spectra and scattering depolarization spectra: The effects of nanoparticle geometry, solvent composition, ligand functionalization, and nanoparticle aggregation. *Analytical Chemistry, 90*(1), 785–793.
Zhou, L., Wang, J. P., Li, D. J., & Li, Y. B. (2014). An electrochemical aptasensor based on gold nanoparticles dotted graphene modified glassy carbon electrode for label-free detection of bisphenol A in milk samples. *Food Chemistry, 162*, 34–40.